

Comparison of the electronic structure of InAs/GaAs pyramidal quantum dots with different facet orientations

Jeongnim Kim,* Lin-Wang Wang, and Alex Zunger
National Renewable Energy Laboratory, Golden Colorado 80401
 (Received 24 December 1997)

Using a pseudopotential plane-wave approach, we have calculated the electronic structure of strained InAs pyramidal quantum dots embedded in a GaAs matrix, for a few height (h)-to-base(b) ratios, corresponding to different facet orientations $\{101\}$, $\{113\}$, and $\{105\}$. We find that the dot shape (not just size) has a significant effect on its electronic structure. In particular, while the binding energies of the ground electron and hole states increase with the pyramid volumes (b^2h), the splitting of the p -like conduction states increases with facet orientation (h/b), and the p -to- s splitting of the conduction states decreases as the base size (b) increases. We also find that there are up to six bound electron states (12 counting the spin), and that all degeneracies other than spin, are removed. This is in accord with the conclusion of electron-addition capacitance data, but in contrast with simple $\mathbf{k}\cdot\mathbf{p}$ calculations, which predict only a single electron level. [S0163-1829(98)50516-4]

Growth of semiconductor quantum dots via controlled coarsening of lattice-mismatched films¹ produces coherently strained islands. These “self-assembled” dots, capped by another semiconductor, exhibit rich spectroscopic features, including explicit evidence of quantum-confinement,² size and shape effects on the spectrum,^{3,4} emission from higher excited states,⁴ interband absorption into up to eight excitonic levels⁵, intraband absorption within the conduction and within the valence bands,⁶ and electron-addition Coulomb blockade.⁷ The shape of these dots, and in particular, the facet orientation, is, however, unclear. For example, for InAs/GaAs, Grundmann *et al.*⁸ reported $\{101\}$ -faceted pyramids, while Nabetani *et al.*⁹ reported pyramids with $\{113\}$ facets, slightly elongated along the $[\bar{1}10]$ direction. In addition, pyramidal shapes with $\{105\}$ facets have been reported by several experiments.¹⁰⁻¹² Often, capping of the dot changes its shape.¹³ Theoretical models of equilibrium facetting¹⁴⁻¹⁷ have not predicted consistently the observed facets, suggesting that perhaps both the kinetic and thermodynamic factors are at play.

Whether the observed facets represent equilibrium conditions or not, the optical and transport properties of the dots must reflect their shapes (thus, the facet orientation) for the following reasons: *first*, the facet orientation determines the smallest dimension (i.e., height) of the dots and therefore the confinement energy of the electronic states. *Second*, different facets correspond to different anisotropic strain inside the dot. *Finally*, different dot shapes have different position-dependent effective masses of electron and holes and different strain-modified band offsets between the dot and its barrier. For these reasons, the energy level structure of dots may depend on *shape*, not just on size. Unfortunately, the shape and size of currently grown “self-assembled” dots is unknown experimentally¹⁻¹³ and theoretically,¹⁴⁻¹⁷ so a direct comparison of calculated energy levels for given size and shape with experimental spectroscopic and transport data is difficult. To address this problem, we study theoretically the electronic structure of InAs square-based pyramidal dots as a function of facet orientation. An important geometrical pa-

rameter of the dots in consideration is the ratio between the height (h) and the base width (b): The pyramidal dots with $\{101\}$, $\{113\}$, and $\{105\}$ facets are characterized by $h/b = 0.5, 0.25,$ and 0.2 , respectively. Thus the higher the facet index, the flatter the dot. In all cases, we assumed that the dot is capped by GaAs barrier and lies on a wetting layer. We use a direct-diagonalization multiband pseudopotential approach¹⁸⁻²⁰ avoiding effective-mass²¹⁻²³ or $\mathbf{k}\cdot\mathbf{p}$ approximations.²⁴⁻²⁶ We uncover the basic trends between various features of the electronic structure and the main geometrical parameters h and b , thus facilitating future comparison with experiments.

The electronic structure of the pyramidal dots is described here using a direct-diagonalization (multiband) approach¹⁸⁻²⁰ to the single-particle Schrödinger equation,

$$\left\{ -\frac{1}{2}\nabla^2 + \sum_{n\alpha} v_{\alpha}(|\mathbf{r} - \mathbf{R}_{n\alpha}|) \right\} \psi_i(\mathbf{r}) = \epsilon_i \psi_i(\mathbf{r}), \quad (1)$$

where v_{α} is a screened empirical pseudopotential of atom type α and $\mathbf{R}_{n\alpha}$ is the position vector of atom type α in cell n . A new strain-dependent pseudopotential is fitted to the measured bulk band structures, hydrostatic and biaxial deformation potentials, and strain-dependent band offsets.¹⁹ We neglect spin-orbit coupling but do not use an effective mass²¹⁻²³ or $\mathbf{k}\cdot\mathbf{p}$ approach²⁴⁻²⁶ in which the microscopic potential $\sum_{n\alpha} v_{\alpha}$ is eliminated and ψ_i is restricted to be described by a few Γ -like bulk states. The atomic positions $\{\mathbf{R}_{n\alpha}\}$ are obtained by minimizing the elastic energy using Keating’s valence-force-field (VFF)^{27,28} model. The resulting system has a C_2 symmetry instead of C_4 . This is because the $[110]$ and $[\bar{1}10]$ directions in the zinc-blend surface are symmetry inequivalent. The single particle wave functions are expanded in a plane-wave basis. We use the “folded spectrum method”²⁰ implemented on a massively parallel computer to find the band edge eigenstates of Eq. (1). The sublinear scaling of this algorithm with the number of atoms allows us to handle systems containing as many as $\sim 10^6$ atoms. We perform supercell calculations with periodic

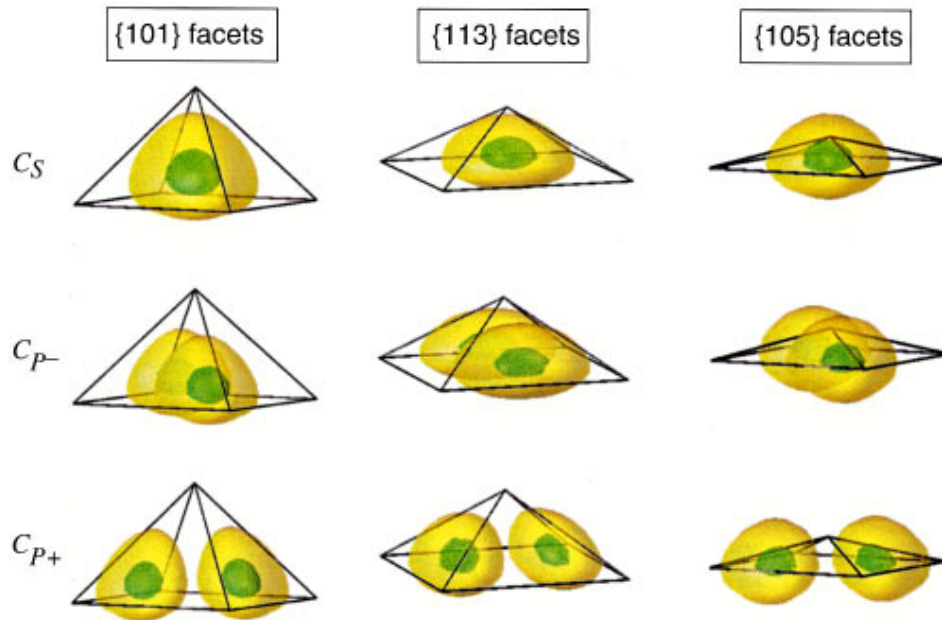


FIG. 1. (Color) Dot confined electron states. Isosurfaces of the three lowest conduction states (yellow at $0.25|\psi_{max}^2|$ and green at $0.75|\psi_{max}^2|$) for pyramidal dots whose base size is 11.3 nm. Relevant energies are given in Table I.

boundary conditions in all three principal directions. We use $[100] \times [010] \times [001]$ supercells for $\{101\}$ and $\{105\}$ pyramids, with a supercell size of $40a \times 40a \times 40a$ (where $a = 5.65 \text{ \AA}$ is the GaAs lattice constant). For the $\{113\}$ pyramids, the $[\bar{1}10] \times [110] \times [001]$ supercell is used with a supercell size of $60a/\sqrt{2} \times 60a/\sqrt{2} \times 40a$. Possible dot-dot interference in the periodic boundary condition has been tested

by changing the size of the supercell, and is found to be very small (causing less than 1 meV eigenvalue differences).

Figure 1 shows the isosurfaces of the three lowest electron wave functions in dots with different facet orientations but with the same base size $b = 11.3 \text{ nm}$. We see that regardless of the facet orientation, the lowest electron state is s -like (C_s). This C_s state is localized mainly inside the dot for

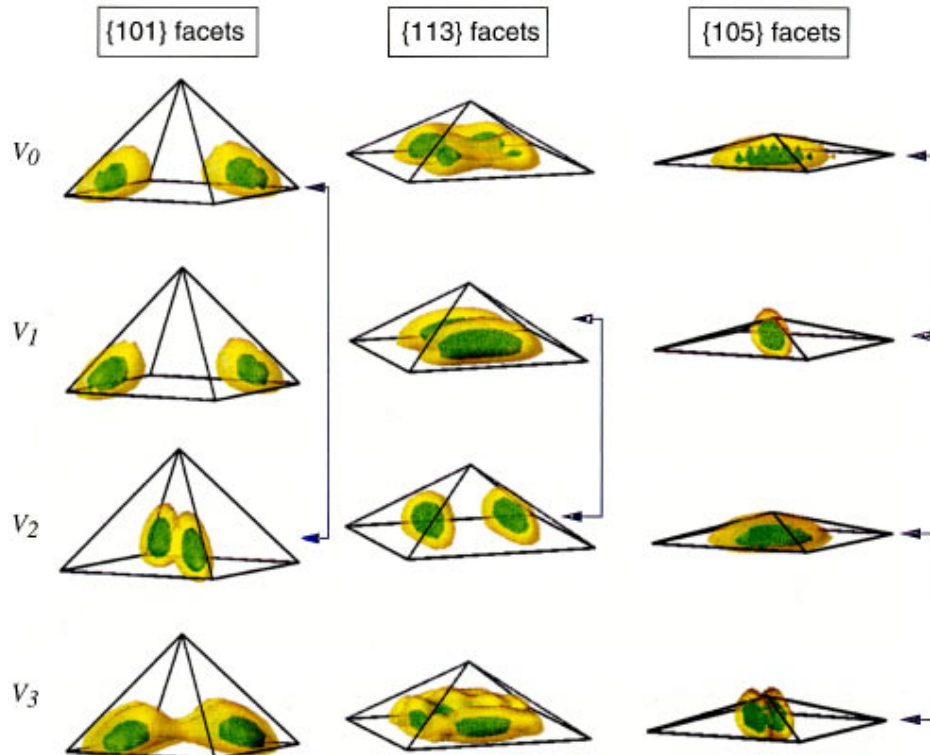


FIG. 2. (Color) Dot confined hole states. Isosurfaces of four highest hole states (yellow at $0.25|\psi_{max}^2|$ and green at $0.75|\psi_{max}^2|$) for pyramidal dots whose base size is 11.3 nm. Pair states that would have been degenerate in C_4 symmetry are connected by arrows. V_1 of $\{101\}$ facet forms a pair with V_4 that is not shown here.

TABLE I. Single particle energies of GaAs-covered InAs pyramids with different facet orientations corresponding to base size b and height h . E_0^v and E_s^c are ground hole and electron state energies, respectively. The dot's single particle band gap is $E_g = E_s^c - E_0^v$. The centroid of the p -like electron states is $\bar{E}_p^c \equiv (E_{p-}^c + E_{p+}^c)/2$. The p -like state splitting is $\delta_p \equiv |E_{p+}^c - E_{p-}^c|$. We also give the number of InAs molecules (N_m) in each dot and the number N_{dot}^c of confined electron states (without counting spin).

| | {101} | | {113} | | {105} |
|---------------------------------------|-------|----------|-------|------|-------|
| b (nm) | 9.0 | 11.3 | 9.0 | 11.3 | 11.3 |
| h (nm) | 4.5 | 5.6 | 2.1 | 2.7 | 1.1 |
| N_m | 3273 | 6171 | 1629 | 3146 | 1603 |
| $E_0^v - E_{vbm}^{bulk}$ (GaAs) (meV) | 265 | 288 | 224 | 244 | 222 |
| $E_s^c - E_{cbm}^{bulk}$ (GaAs) (meV) | -177 | -231 | -119 | -177 | -94 |
| E_g (eV) | 1.08 | 1.00 | 1.17 | 1.10 | 1.20 |
| $\bar{E}_p^c - E_s^c$ (meV) | 113 | 97 | 100 | 95 | 72 |
| δ_p (meV) | 28 | 27 | 9 | 9 | 5 |
| N_{dot}^c | 3 | ≥ 5 | 3 | 4 | 3 |

{101} and {113} faceted dots, while it also has significant amplitude in the barrier for the {105} faceted dots. The shape of the C_s states is slightly elongated along the [110] direction due to the C_2 symmetry of the dot. The second and third lowest conduction states form a nondegenerate pair, characterized by a single nodal plane, either in the {110} or in the $\bar{1}\bar{1}0$ plane passing through the center. We denote the p -like state with the {110} nodal plane as $C_{p-} = p_x - p_y$, and the p -like state with the $\bar{1}\bar{1}0$ nodal plane as $C_{p+} = p_x + p_y$. In C_4 symmetry assumed in previous nonatomistic continuum calculations,²¹⁻²⁵ this p -like pair would have been unphysically degenerate. Our calculation predicts that all spatial degeneracies are removed. We denote the splitting of C_{p-} and C_{p+} as $\delta_p = |E_{p+}^c - E_{p-}^c|$ and the centroid of their energies as $\bar{E}_p^c \equiv (E_{p-}^c + E_{p+}^c)/2$. Table I gives the position of the C_s and C_p state, the p state splitting δ_p , the valence state energy E_0^v , the band gap $E_g = E_s^c - E_0^v$, and the number N_{dot}^c of the confined electron states.

Figure 2 shows isosurfaces of four highest *hole* wave functions. We see that hole states tend to be more confined inside the dot and more compact than the electron states. The symmetry and shape of hole states is different for different facet orientations. We do not find localization of the hole wave functions along the pyramidal edges or around the pyramidal tips as found in previous $\mathbf{k} \cdot \mathbf{p}$ calculations.²⁴ As is the case for the C_{p-} and C_{p+} *electron* states, pairs of states also exist for the *hole* states, as shown (by arrows) in Fig. 2. For example, V_0 and V_2 for {101} faceted dots form a pair, in that they would have been degenerate in C_4 symmetry. The hole states do not have the simple symmetries obtained in continuum approximations.²¹⁻²⁵ This is because in our calculation a *few* Bloch states are allowed to couple in forming the dot states (other calculations restrict the coupling) and because of the existence of inhomogeneous strain.

The main trends in the energy level structure in relation to the basic geometrical parameters of the pyramidal dots are the following:

(i) There are as many as six confined electron states (12 states if the spin is counted), N_{dot}^c , in the largest {101} dot

we have investigated. The N_{dot}^c decreases as the facet orientation goes to {105}. The existence of more than one electron state agrees with recent electron-addition capacitance experiments showing three or more excited electron states. It disagrees with $\mathbf{k} \cdot \mathbf{p}$ calculations²⁴ predicting a single confined electron state.

(ii) The binding energy of the s -like conduction state, $|E_s^c - E_{cbm}(\text{GaAs})|$, and the binding energy of the highest hole states, $E_0^v - E_{vbm}(\text{GaAs})$, both increase with the number N_m of InAs molecules in the dot (i.e., the volume b^2h of the dot). Therefore, the same is true for the band gap, $E_g = E_s^c - E_0^v$.

(iii) The s - p energy difference, $\bar{E}_p^c - E_s^c$ (between the center of the electron p doublet and the lowest electron s state) decreases as the *base size* b increases.

(iv) The splitting δ_p between the two p -like conduction states increases with the *facet orientation* h/b , and is almost independent of the dot size for fixed facet orientation. Thus measurement of δ_p could be used to assess the facet orientation.

(v) The change ΔE_{VB} of the hole binding energies with dot sizes is, however, weaker than the change ΔE_{CB} of the electron binding energies with the dot size. The overall change in band gap is distributed as $\Delta E_g \sim 2/3 \Delta E_{CB} + 1/3 \Delta E_{VB}$.

(vi) We find many confined hole states (>6 without counting spin) for all the dots we have investigated. The energy splittings between nearest hole states²⁹ are of the order of a few meV, much smaller than the s - p splitting $\bar{E}_p^c - E_s^c$ of the electron states.

As indicated by (ii), the energy gap decreases as the dot volume increases, irrespective of shape. The energy gap of the dots containing about 3000 InAs molecules is 1.1 eV, in good agreement with the experimental gaps of similar size dots.^{4,10,16} Our calculation agrees well with the capacitance measurements in the presence of the magnetic fields by Miller *et al.*⁷ in that there are as many as six dot electron states (counting the spin up and down degree of freedom) for the large dots. The symmetries of the three lowest conduction states also agree with those identified by these authors. We estimate from (iii) $\bar{E}_p^c - E_s^c \approx 50$ meV at $b = 20$ nm for {113} facet. This equals the experimental value⁴ (50 meV) for the same base size quantum dot.

There are two conflicting views in interpreting the photoluminescence (PL) spectra: Model²⁴ A suggests that the PL involves transitions from the ground electron state C_s (the only confined electron state²⁴) to the ground hole state V_0 and to the excited hole states³ $V_1 \cdots V_3$. Model⁴ B suggests that the PL spectra are due to the ground electron-hole transitions ($C_s - V_0$) and excited electron-hole transitions ($C_p - V_1$). From our calculated results, we see that if the splitting of PL peak was due to different hole state, it would only be about a few meV, much smaller than the experimental values. Thus, we attribute the experimentally observed PL peaks to the splitting of electron states. Note that in model B $C_s - V_1$ is predicted to be forbidden.

Figure 3 shows a few possible optical transitions involving the three lowest conduction states, C_s , C_{p-} , and C_{p+} , and a few highest hole states for the dot with $b = 11.3$ nm and different orientations. We define the dipole moments as

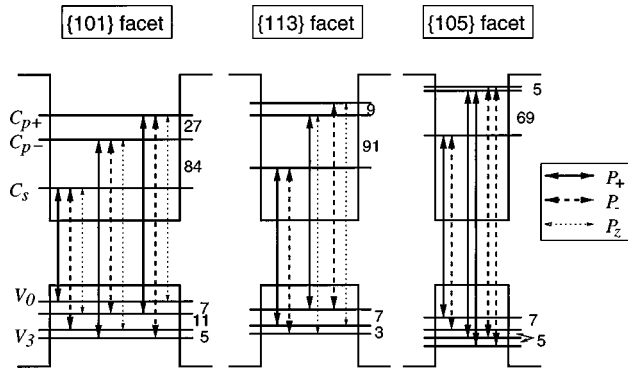


FIG. 3. Allowed dipole transitions connecting the three lowest conduction states and a few highest valence states. The energy differences between the neighboring states are given in meV. The P_+ , P_- , and P_z indicate the transition polarizations.

$P_+ = \langle C_i | P_x + P_y | V_j \rangle$, $P_- = \langle C_i | P_x - P_y | V_j \rangle$, and $P_z = \langle C_i | P_z | V_j \rangle$, where x, y and z denote the $[100]$, $[010]$, and $[001]$ directions, respectively. We find the following:

(a) For the $\{101\}$ faceted dots, the transitions from the ground electron state C_s to the ground hole state (V_0) and to the excited hole states (V_1 and V_2) are allowed. Their transition dipole moments strongly depend on the polarization: the $C_s \rightarrow V_0$, $C_s \rightarrow V_1$, and $C_s \rightarrow V_2$ transitions are allowed for polarization P_+ , P_z , and P_- , respectively.

(b) For the $\{113\}$ faceted dots, the transition from C_s to V_0 is forbidden (dark exciton), while it is allowed for $\{101\}$ and $\{105\}$ faceted dots.

(c) There are no dipole-allowed transitions polarized along the z direction (P_z transitions) for the flatter $\{105\}$

faceted dot. On the other hand, we find three transitions, $C_s \rightarrow V_1$, $C_{p-} \rightarrow V_3$, and $C_{p+} \rightarrow V_0$, that are polarized along z direction for the $\{101\}$ faceted dot.

(d) Due to the C_2 symmetry, transitions from C_s to the pair hole states connected by arrows in Fig. 3 are allowed and activated by different polarizations, e.g., for the $\{105\}$ faceted dot, PL signals by transitions from C_s to V_0 and V_1 are polarized along the P_+ and along the P_- , respectively.

(e) Transitions from the pair p -like conduction states to a hole state are activated by different polarizations. For instance, transitions $C_{p-} \rightarrow V_0$ and $C_{p+} \rightarrow V_0$ of the $\{113\}$ faceted dot are both allowed but are activated by different polarizations.

In summary, we have compared the electronic structures of strained InAs pyramidal dots embedded in GaAs with different facet orientations. Our calculations show that an accurate description of the atomistic potential, inhomogeneous strain, and multiband couplings are crucial in determining the symmetry and shape of the conduction and hole wave functions. The calculations provide important trends of the binding energies, band gaps and level splittings, in regard to the facet orientations.

The authors would like to thank P. M. Petroff, K. H. Schmidt, D. Bimberg, A. Madhukar, and O. Stier for helpful discussions of the experimental data. This work was supported by the United States Department of Energy-Basic Energy Sciences, Division of Materials Science, under Contract No. DE-AC36-83CH10093. The computational aids were provided by the National Energy Research Scientific Computer Center (NERSC).

- *Present address: Dept. of Physics, OSU, Columbus, OH 43210.
¹W. Seifert *et al.*, Prog. Cryst. Growth Charact. Mater. **33**, 423 (1996).
²G. Medeiros-Ribeiro, F. G. Pikus, P. M. Petroff, and A. L. Efros, Phys. Rev. B **55**, 1568 (1997).
³J. Grundmann *et al.*, Phys. Rev. Lett. **74**, 4043 (1995).
⁴K. Schmidt *et al.*, Phys. Rev. B **54**, 11 346 (1996).
⁵R. Heitz *et al.*, Appl. Phys. Lett. **68**, 361 (1996).
⁶S. Sauvage, *et al.*, J. Appl. Phys. **82**, 3396 (1997).
⁷B. T. Miller *et al.*, Phys. Rev. B **56**, 6764 (1997).
⁸S. Ruvimov *et al.*, Phys. Rev. B **51**, 14 766 (1995).
⁹Y. Nabetani *et al.*, J. Appl. Phys. **76**, 347 (1994).
¹⁰Q. Xie *et al.*, J. Cryst. Growth **150**, 357 (1995).
¹¹G. S. Solomon, M. C. Larson, and J. S. Harris, Appl. Phys. Lett. **69**, 1897 (1996).
¹²H. Lee *et al.*, Appl. Phys. Lett. (to be published).
¹³J. M. Garcia *et al.*, Appl. Phys. Lett. **71**, 2014 (1997).
¹⁴J. Tersoff and F. LeGoues, Phys. Rev. Lett. **72**, 3570 (1994).
¹⁵C. Priester and M. Lannoo, Phys. Rev. Lett. **75**, 93 (1995).
¹⁶V. Shchukin *et al.*, Phys. Rev. Lett. **75**, 2968 (1995).
¹⁷N. Moll *et al.*, Phys. Rev. B **54**, 8844 (1996).
¹⁸A. Zunger, MRS Bull. **23**, 35 (1998); A. Williamson, A. Zunger, and A. Canning, Phys. Rev. B **54**, R4253 (1998).

- ¹⁹J. Kim, A. Williamson, L. W. Wang, S. H. Wei, and A. Zunger (unpublished). The empirical pseudopotential in reciprocal space is given by $V_2(q) = [1 + a_{42} \text{Tr}(\epsilon)] a_{02} (q^2 - a_{12}) / \times [a_{22} \exp(a_{32} q^2) - 1]$, where ϵ is the local strain tensor. In atomic units, the parameter $\{a_{02}, a_{12}, \dots, a_{42}\}$ are $\{55.738, 2.793, 3209, 0.2830, 1.863\}$ for Ga; $\{107.76, 1.915, 3.460, 0.414, 1.665\}$ for In; $\{48.54, 2.536, 1.463, 0.4937, 0.0\}$ for As in GaAs; $\{49.61, 2.736, 1.523, 0.5744, 0.0\}$ for As in InAs.
²⁰L.-W. Wang and A. Zunger, J. Chem. Phys. **100**, 2394 (1994).
²¹J.-Y. Marzin and G. Bastard, Solid State Commun. **92**, 437 (1994).
²²L. R. C. Fonseca, J. L. Jimenez, J. P. Leburton, and R. Martin (unpublished).
²³A. Wojs *et al.*, Phys. Rev. B **54**, 5604 (1996).
²⁴M. Grundmann, O. Stier, and D. Bimberg, Phys. Rev. B **52**, 11 969 (1995).
²⁵M. A. Cusack *et al.*, Phys. Rev. B **54**, R2300 (1996).
²⁶H. Jiang and J. Singh, Phys. Rev. B **56**, 4696 (1997).
²⁷P. Keating, Phys. Rev. **145**, 637 (1966).
²⁸J. L. Martins and A. Zunger, Phys. Rev. B **30**, 6217 (1984).
²⁹The shape of the wave functions and the order of levels for hole states are found to depend sensitively on the size of the dots and on the local strain. Inclusion of spin-orbit coupling can further change the deep hole states.